A Field-Deployable Wireless Data Acquisition System for Ground-Test Arrays

William C. Patterson[1], James R. Underbrink[2], Rachel Collins[3], Austin Kee[4], Alan Gurlaskie[5], Dan D'Andrea[6], David A. Mills[7]
Interdisciplinary Consulting Corp, Gainesville, FL 32609

William M. Humphreys, Jr.[8]
NASA Langley Research Center, Hampton, VA 23681

This paper describes the development, characterization, and deployment of a field-deployable wireless data acquisition system for ground-test arrays, applicable in noise-source localization or beamforming measurements such as those encountered during airframe noise flyover measurement tests. The system design is enabled by commercially available, low-power Internet of Things (IoT) processors and Wi-Fi communication components. Time is synchronized across the array wirelessly by leveraging the Coordinated Universal Time (UTC) provided by the Global Positioning System (GPS). Initial laboratory characterization of the system demonstrated its ability to meet acoustic bandwidth, dynamic range, time synchronization, environmental, and battery life requirements for typical ground-test array deployments. A successful system deployment at NASA Langley was performed that included measurement of a suspended elevated static noise source, and Uncrewed Aerial System (UAS) vehicle measurements using a quadcopter operated both in hover mode and forward flight. Beamform analysis of the acquired data showed an excellent ability of the array to extract accurate sound pressure levels from the suspended source. Synchronization of the array and vehicle GPS timecodes allowed the ability to extract acoustic signatures from the UAS vehicle during hover and forward flight maneuvers over the array. These results validate the use of high-channel count wireless arrays in airframe noise flyover test campaigns.

I. Nomenclature

ADC = Analog-to-Digital Converter
ARM = Advanced RISC (Reduced Instruction Set) Machine
COTS = Commercial-off-the-shelf
DAQ = Data Acquisition System
GPS = Global Positioning System
GUI = Graphical User Interface
LiPo = Lithium Polymer
MEMS = Microelectromechanical Systems
PoE = Power over Ethernet
REST API = Representational State Transfer Application Program Interface(API)
RTK = Real-Time Kinematic
TSM = Time Synchronization Module
UTC = Coordinated Universal Time
VCTCXO = Voltage Controlled Temperature Compensated Crystal Oscillator
WAP = Wireless Access Point

---

[1] Vice President, Principal Engineer, Interdisciplinary Consulting Corp (IC2)
[2] Senior Technical Fellow, Interdisciplinary Consulting Corp (IC2), AIAA Associate Fellow
[3] Electrical Engineer, Interdisciplinary Consulting Corp (IC2)
[4] Embedded Electrical Engineer, Interdisciplinary Consulting Corp (IC2)
[5] Electrical Engineer, Interdisciplinary Consulting Corp (IC2)
[6] Senior Embedded Software Engineer, Interdisciplinary Consulting Corp (IC2)
[7] Principal Engineer, AIAA Member
[8] Chief Engineer for Measurement Sciences, Research Directorate, AIAA Associate Fellow

II. Introduction

As higher-efficiency aircraft variants that are tailored for specific routes continue to flourish, full-scale tests will become ever more necessary to continue to lower the noise emissions of commercial flights. As cities continue to increase in size and creep towards the land surrounding airports, and as overall air traffic continues to increase, noise regulations will become more restrictive. This will require precise identification of the main noise contributors of an aircraft during takeoff and landing to prevent invasive noises to the surrounding communities. Although likely noise sources can be located and tested using scale models in wind tunnels, only in full-scale tests are accurate Reynolds numbers and complex geometries present during take-off and landing configurations to provide accurate airframe, engine, and component interaction noise generation data. Airframe noise measurement and source localization are extremely well suited for large, field-deployed microphone phased arrays. Also, with the resurgent push to make overland supersonic aircraft possible, measurements of the highly complex sound interactions of full-size vehicles will be required to make 'Low-Boom' aircraft a reality [1]. Extremely large arrays are desired for understanding the propagation and effects at ground level of sonic booms.

Full-scale fly-over tests, however, are complicated and expensive (albeit necessary) methods to meet community noise regulations. Even with these expenses, the number and frequency of community noise flyover "technology" tests has increased in recent years in the U.S. (NASA, FAA, and Boeing) [2–6], in Europe, and in Japan, as a means of validating new technologies and advancing the Technology Readiness Level (TRL) to accelerate adoption of these technologies into commercial products. Microphone phased arrays have become an integral part of these test campaigns.

The current state of the art for field-deployed microphone phased arrays uses centralized data acquisition systems, electret-type microphones with varying microphone preamplifiers and various cabling schemes to connect the microphones back to the central system, usually in a star configuration. NASA Langley has published a microphone array with a 250 ft. diameter and 186 microphones. The system requires a special amplifier board at each microphone to drive a 400 ft. cable [2] as well as a large single-purpose data acquisition system that is cable-limited in the distance it can be located away from the array to minimize acoustic reflections and interference. In the commercial sector, The Boeing Company has published and performs ground tests with a 288.5 ft. diameter array of 840 microphones, with 555 of those being satellite nodes [4]. Traditional wired microphone ground-test arrays are size and channel-count limited due to the procurement and deployment costs associated with a wired data system as well as the pragmatic physical limitations on array aperture size associated with a wired solution.

The wireless ground-test array system presented herein addresses the size and deployment cost limitations of these traditional wired systems by leveraging the flourishing Internet-of-things (IoT) movement that provides instrumentation engineers with lower-cost and higher-performance sensors and computing systems due to economies of scale. The system takes full advantage of newly available MEMS microphones, analog-to-digital converters, single-board computers, positioning systems, and power systems. For a reduced system cost compared to a traditionally wired array, the proposed system provides more advanced sensors and computational processing directly at the node endpoint. The localized computational processing allows for increased signal acquisition fidelity, environmental compensation, and the benefit of lossless data transmission through the digital domain. Also, due to the wireless nature of the system, deployment time and costs are drastically reduced. The system enables accelerated deployment, increased size and microphone count, lower cost, and higher performance when compared to traditionally built wired arrays. Furthermore, this technology allows the array to grow nearly linearly in hardware cost and deployment labor for both array microphone count and spatial size. This contrasts with the significant cost increases associated with wired systems as they increase in channel count and spatial extent since cable lengths need to be extended and kept at the same length for every channel in order to maintain channel-to-channel phase matching. This new wireless system not only enables more extensive array deployments at a reduced cost, but may also increase the number of deployments for full-scale air-frame noise source testing and engine stand testing due to the higher fidelity measurements that may be achieved at a significantly lower deployment cost.

Complete characterization of the wireless array system is presented, including acoustic performance of the microphone, synchronization performance of the wireless channels, and environmental robustness of the system. Also, the system was deployed at a NASA facility and tested with a static elevated acoustic source, and a quadcopter flyover aircraft. Beamform analysis of the acquired data showed an excellent ability of the array to extract accurate sound pressure levels from the suspended source. Synchronization of the array and vehicle GPS timecodes allowed the ability to extract acoustic signatures from the UAS vehicle during hover and forward flight maneuvers over the array. These results validate that the use of a high-channel count wireless array is advantageous in airframe and propulsion noise flyover test campaigns.

III. The Wireless Data Acquisition System

The system consists of three major components: the acquisition nodes, the data-collection network, and the data-collection and hardware orchestration software. A representative diagram of the system is shown in Fig. 1. There are two types of nodes in an array – a large central fixed plate array, and individual ‘satellite’ nodes. The central plate is a densely packed array of microphones permanently installed into a stiff flat structure, which provides the following benefits: (1) the relative microphone locations are defined by machining tolerances; and (2) the microphones can be prewired and installed in the central plate prior to array deployment. The large arms of an array are composed of single-microphone ‘satellite’ nodes. Each of the ‘satellite’ nodes is a self-sufficient, environmentally hardened system capable of providing excitation, signal conditioning, and digital data from an analog (microphone) signal, time-syncing with other systems, storing and transmitting requested data, and managing its own power system. The ‘network’ consists of environmentally hardened COTS networking components that transmit commands from the client to the nodes and collect data from the nodes to return to the client. The orchestration software manages the data acquisition, collection, and storage process.

The prototype demonstration array is a reduced adaptation of a NASA Langley 185 microphone wired array [4]. This array consists of 73 total microphones, with 37 microphones in the central plate and 36 satellite nodes in 3 rings of 12 nodes. The array covers an approximately 50 ft. diameter circle, and the microphone positions were optimized for testing over a 44.7 Hz to 11.2 kHz acoustic bandwidth. A summary of the key technical requirements aimed to be achieved by the system are shown in Table 1.

Table 1 Summary of key requirements for wireless array system.

	Requirement
Acoustic	
Freq. Resp (3db):	44.7 Hz to 11.2 kHz
Upper Range:	128 dBSPL @ 3% THD
Dynamic Range:	75 dBSPL
Amp. Accuracy:	±0.3 dBSPL
Phase° Uncert.:	7° @ 11.2kHz or 1.7 µs
Data Acquisition	
Sample Rate:	>40 kS/s
Sampling Synch:	<100 ns
Data Storage:	10 runs @ 30 s/run
Communications	
Wireless Range:	15 m
Data Upload Speed:	<1 s after request per 30 s run
Power:	
	50x 30s runs/day for >3 days
Enclosure And Env.	
Size:	< 18 cm in dia., < 8 cm height
IP Rating:	IP65
Operating Temp:	0 - 60°C humidity 20-90%

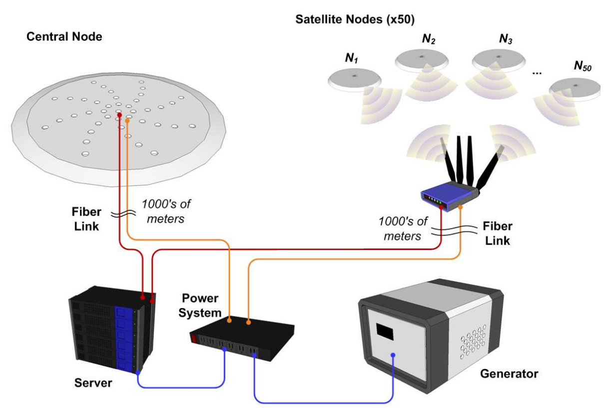

Fig. 1 Schematic of proposed network topology consisting of a central plate with many microphones, many single-microphone satellite nodes, wireless access points, and a control system consisting of a server, system power control, and a power source/generator.

A. The Satellite Node

The satellite nodes are all identical and can be placed anywhere in an array design. It should be noted that the electronics in the central plate are identical to satellite nodes electronics except that unnecessary components have been removed, i.e., battery power, wireless systems, etc. The satellite node consists of three main subsystems: (1) the communication module; (2) the data acquisition module; (3) and the time synchronization module. They are arranged according to the block diagram shown in Fig. 2(b). The communication module is responsible for network (wireless and ethernet) communication, power system control, system configuration and management, data storage, and user communication. The data acquisition module is responsible for the analog front end and microphone module control, ADC control and acquisition, synchronization for sample alignment, and data buffering for the communication processor. Finally, the time synchronization module oversees: GPS control and communication, VCTCXO oscillator tuning and phase locking, the trigger alarm system, and the 10 MHz system clock.

Each of these subsystems exist on either the main motherboard or a daughterboard. Also included in the satellite node enclosures are a LiPo battery, solar cells, an environmentally hardened microphone module, and a charging interface. An exploded view of the system is shown in Fig. 2(a).

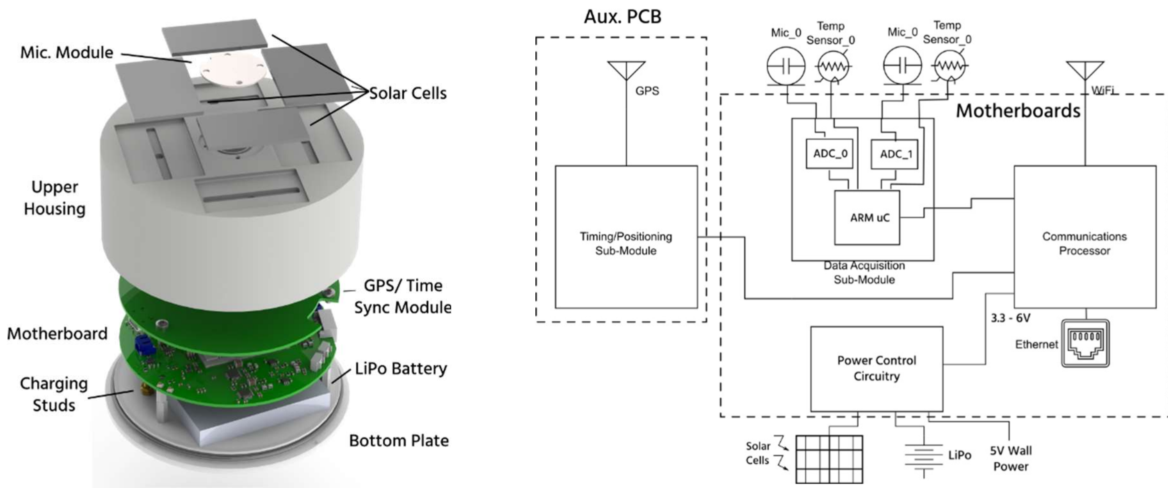

(a) (b)

Fig. 2 (a) Exploded view of satellite node, and (b) a block diagram of a satellite node design.

1. Time Synchronization Module (TSM)

The TSM subsystem is responsible for proving the ADCs with a 10 MHz clock signal that is synchronized across all nodes. The TSM also provides a wireless trigger system to start all the ADCs, similar to a traditional trigger line used on benchtop equipment, but without a wired connection. This system functions by receiving a GPS satellite atomic clock signal through a GPS receiver and synchronizing an internal RTC and 10 MHz oscillator to the GPS signal. The internal oscillator allows the system to stay well within the synchronization requirements even if the GPS signal is lost momentarily due to cloud cover. Fig. 3 shows the phase delay error of two separate, unconnected TSMs as they are started from a cold start. In about six minutes they are synchronized to one another to within 40 ns.

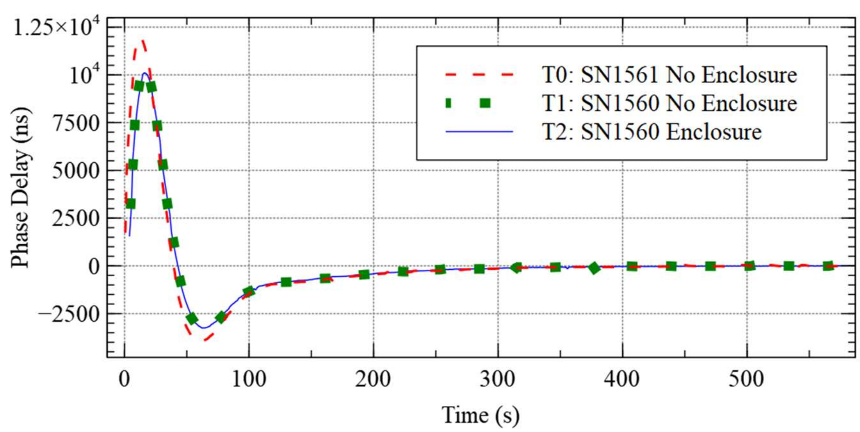

Fig. 3 Comparison of two different time synchronization modules outside of and within an enclosure (enclosure does not make a detectable difference).

2. The Data Acquisition Module

The data acquisition subsystem consists of a 32-bit ARM processor and is responsible for managing the ADCs and buffering data to be sent to the communications processor for storage. The ADC is a 24-bit, fully differential delta-sigma with a 115.5 dB signal-to-noise ratio (SNR) at a 62.5 kS/s sample rate. Also included are anti-alias filters with -1 dB @ 61 kHz to ensure a flat frequency response (further anti-aliasing is provided by the delta-sigma oversampling) and a phase shown in Fig. 4(a).

3. The Environmentally Hardened Microphone Module

The environmentally hardened microphone module is connected to the data acquisition module as shown in Fig. 4(b). This field-swappable module includes an IP56 MEMS microphone and a temperature sensor, allowing the system to remain protected from the weather through the entirety of deployments, minimizing labor requirements typically needed by previous systems to uncover and recover the microphones each day. The temperature sensor allows for the end-user to perform temperature compensation of the acquired data if desired.

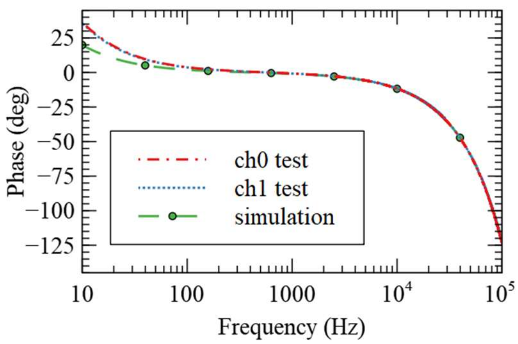

(a)

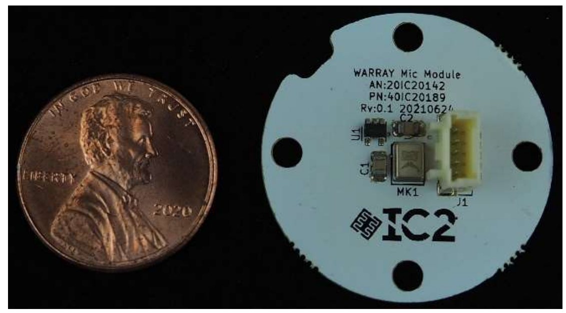

(b)

Fig. 4 (a) Phase response of DAQ subsystem. (b)MEMS microphone module.

4. The Central Processing System

The central processing system consists of an ARM processor running a custom-built Linux distribution, with custom drivers for all the hardware interfaces. This system oversees controlling the TSM and DAQ systems and communicating with the end-user over Wi-Fi and/or ethernet connection. The system is also responsible for the control of the power system, which can monitor the power supplies and battery life, enable/disable subcomponents, and put the system into sleep mode to conserve battery power. Finally, the system provides two internet-connected interfaces for interacting with each node. The first is a REST API interface that allows all the functions of the node to be programmatically controlled. This is the method by which a full array of nodes is controlled with the orchestration software. The second is a web GUI that is available for interfacing with a single node in case specific configuration or monitoring is desired. This web GUI provides the user with functionality such as checking status, functionality, power-up and -down, and setting system parameters. A screen shot of the prototype web GUI is shown in Fig. 5.

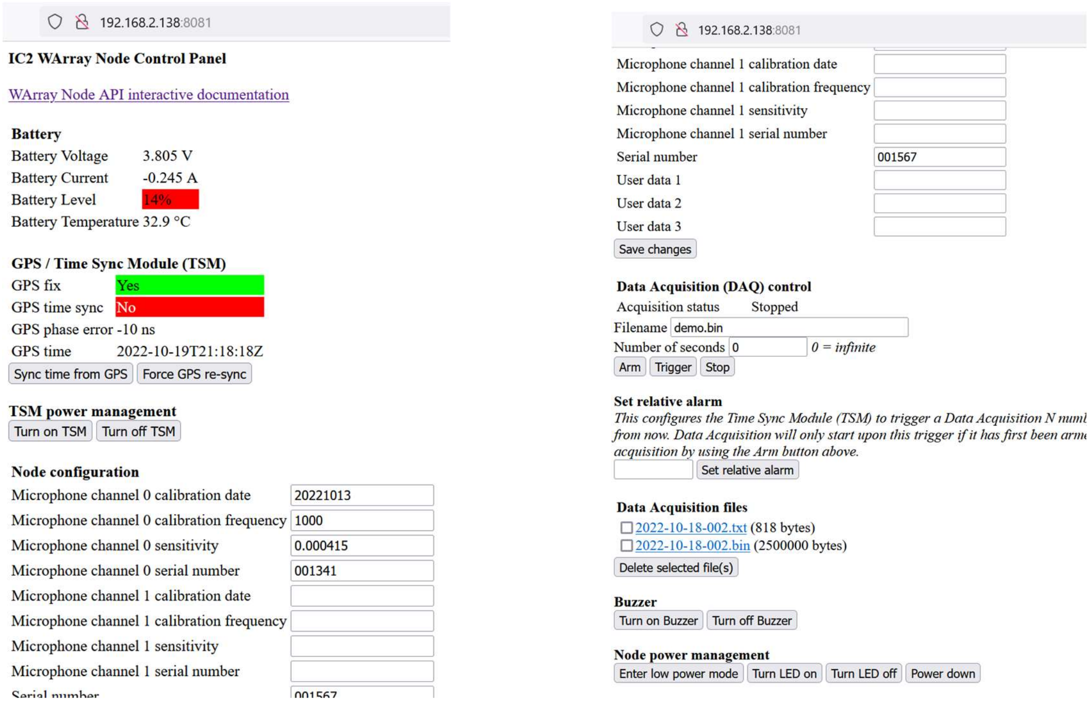

(a) (b)

Fig. 5 Web GUI single node interface. (a) Top of page, (b) Bottom of page.

5. *The Enclosure*

The satellite node enclosure, shown in Fig. 6, is designed to provide a waterproof housing for the electronic components, and a sound hard surface for mounting the microphone. The dimensions of the enclosure were optimized to increase close packing density of satellite nodes, thus minimizing the total size required for a central plate. The final dimensions of each node are 113 mm [4.4 in] diameter and 55 mm [2.1 in] height. The enclosure also includes a gasketed and removeable microphone module, top-embedded solar panels, a waterproof main enclosure with a magnetically actuated power switch, dual purpose mounting/charging studs on the bottom, a disposable mounting plate (meant to be adhered to the installation surface), and a removeable acoustic fairing (not shown in the figure).

(a) (b)

Fig. 6 Satellite node enclosure design. (a) exploded view of CAD design. (b) final assembled enclosure (sans fairing).

B. The Central Plate

To resolve higher frequency components of sound sources, a higher density of microphones with higher precision positioning is required. Due to these constraints, it is more efficient to build a large central plate than multiple satellite nodes. The central plate consists of many of the same electronic systems found in the satellite nodes with the differences being: each node acquires two channels of audio input; communication is through ethernet rather than Wi-Fi; a single TSM triggers all channels; and all electronics are powered off an external DC power supply. The block diagram of the central plate design is shown in Fig. 7.

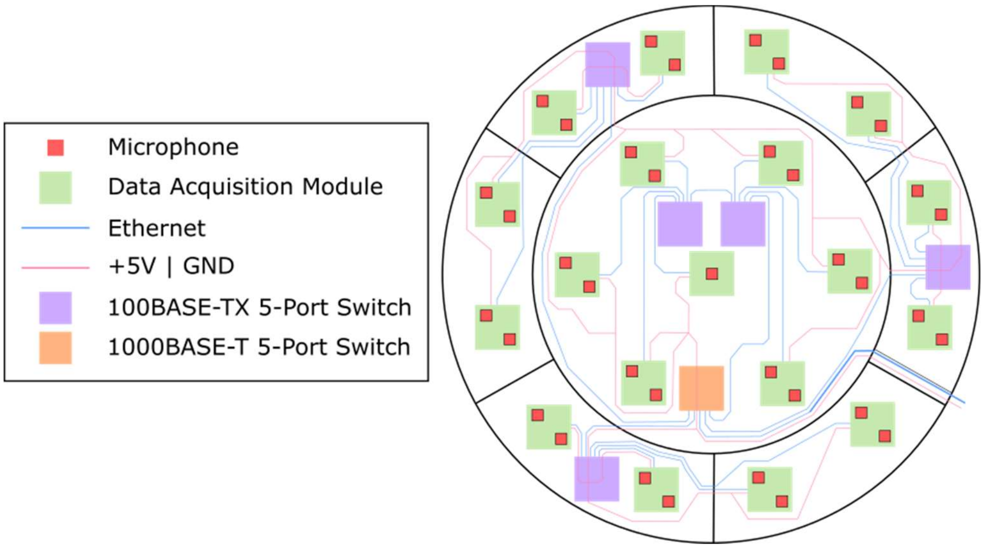

Fig. 7 Block diagram of central plate electronic submodules and interconnection.

The central plate enclosure, shown in Fig. 8, consists of four subparts: a frame, a central enclosure module, six auxiliary ‘petal’ enclosure modules, and six corresponding fairing components. The frame of the central plate is made of two halves to minimize the total size for transportation and assembly. In larger designs the frame would be divided into even more sections. The central and petal modules are self-contained inserts that are installed into the frame structure. Each module is composed of three parts: a top plate, a gasket seal, and a tub. The design allows each central plate module to be replaced in the field while maintaining waterproofing and avoiding disassembly of the central plate. Additionally, the internals of each of the waterproofed modular enclosures can be accessed from the top with only a screwdriver if further repair is required on a fully assembled central plate.

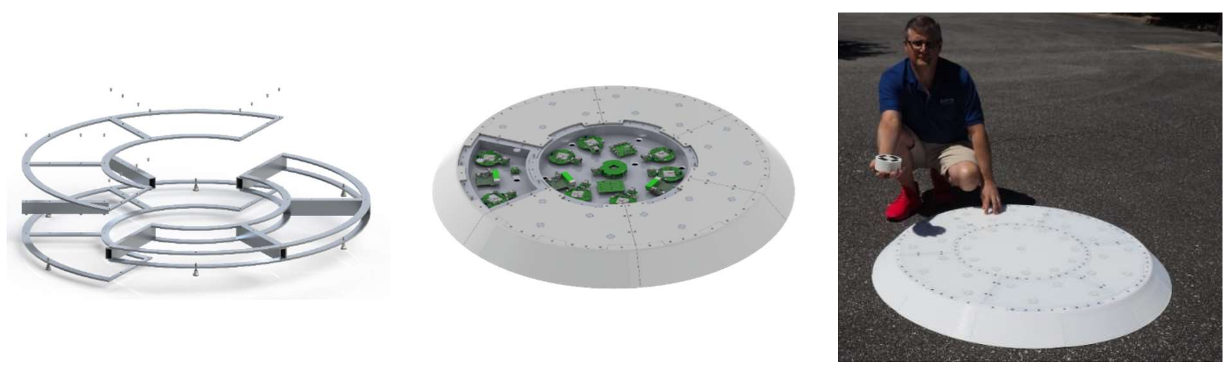

(a) (b) (c)

Fig. 8 (a) Central plate frame exploded view. (b) central plate partial exploded view. (c) central plate with satellite node.

C. The Network Hardware and Orchestration Software

1. *Network Hardware*

The network hardware is designed to leverage widely available industrial-rated COTS networking and wireless equipment. This allows for the system components to be highly performant and flexible with respect to cost. For a larger array with more nodes, the system would be equipped with higher speed network hardware and more WAPs. The network hardware consists of control center hardware and runway network hardware.

The control center hardware consists of a laptop, a router, and a 120V power supply. A laptop with a standard Microsoft Windows operating system is used to run the orchestration software. A standard laptop has sufficient processing power to control even a massive array, because the software performs most operations round-robin or in small parallel groups, thus eliminating the need for more exotic, high-bandwidth server hardware. For the runway network hardware, a small, low-cost gigabit router is used to assign IPs to each connected node over a standard small form pluggable (SFP) networking port to allow for a fiber transceiver when long cable runs are required from the control center to the runway. An AC power source is required to power the control center and the runway equipment. It was found that a 1000 W/hr LiPo battery bank/inverter with a solar panel was sufficient for the test deployment's day-to-day power requirements.

A custom NEMA-rated enclosure, shown in Fig. 9, with waterproof bulkhead connections, is placed near the central plate (within 20 ft). This enclosure requires 120/240V AC power supplied from the control center. The AC power is used for the central plate AC to DC power supply. By separating the AC to DC power supply from the central plate, significant 60Hz noise was eliminated. The enclosure also contains an industrial-rated PoE network switch. This network switch provides: a network connection from the control center to the central plate; and the network connectivity and power to the PoE WAPs. Two PoE WAPs were wired through ethernet to tripods located at the perimeter of the array to supply network connectivity to the satellite nodes.

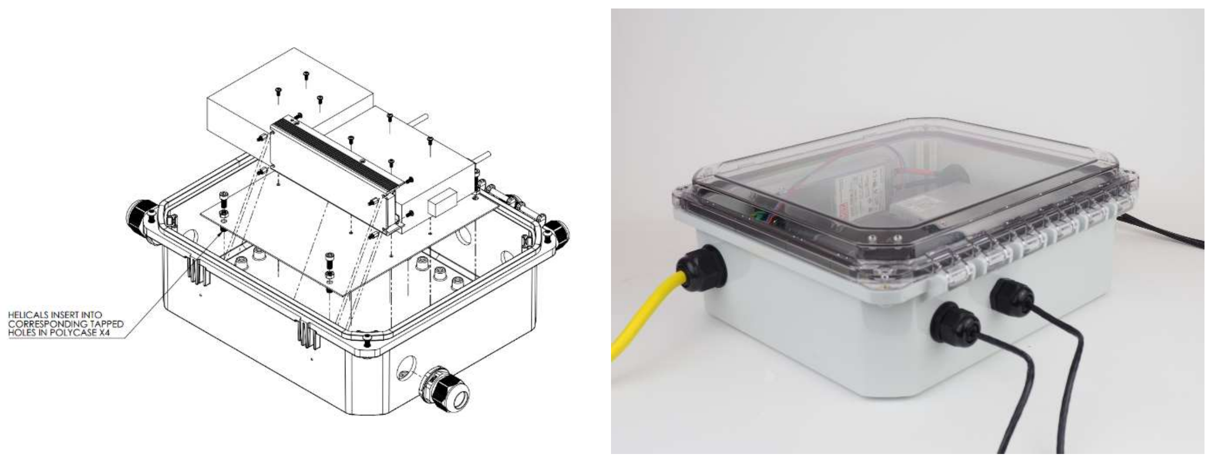

(a) (b)

Fig. 9 (a) Enclosure CAD model, and (b) final assembled enclosure.

2. Custom Software

The orchestration software used to simultaneously control all the nodes during an array deployment consists of a single executable that can be run on a standard laptop. The software user interface consists of five tabs, or sections, that are used for different stages of the deployment.

The 'Node Placement' tab allows the end-user to upload a CSV file containing the local X and Y coordinates and serial numbers for the nodes. This tab is used for initial loading of the nodes into the software, and it will also export the CSV file, post array installation, with the record of the nodes placement and the coordinates from the final node surveying.

The 'Node Map' tab provides a graphic display of the previously uploaded CSV file. This can help with deploying a node to its specific location and for locating nodes in a large array, needed for example, when calibration or troubleshooting are required. This interface also allows the tracking of placed nodes during deployment, and, if a node is double-clicked, it will open the node's web GUI interface for direct interfacing.

The 'Node Control' tab allows the orchestration software to scan the network for all available nodes and add them to the control list. Once the list of controllable nodes is complete, this tab allows the end user to send out commands and receive responses from all nodes and/or a subset of those nodes simultaneously. This tab is very useful for checking the status of nodes such as battery level, GPS, and time sync status. This tab is also used to power down the entire system at the end of a day of data acquisition.

The 'Data Acquisition' tab, shown in Fig. 10, is the portion of the program used during flight testing operations, after the nodes have been confirmed as 'up' and functional. The system provides a 'Node Health' check that runs through a suite of tests on all nodes, such as GPS sync status and battery health, to ensure all nodes will acquire data successfully. Then the acquisition length in seconds and the filename for an acquisition can be input by the user and sent to all nodes. A start button will then command all the nodes to start acquiring data 5 seconds from the time the button is pressed. Future revisions of the software will allow for instantaneous triggering.

After one or more acquisition events, the 'File Management' tab is used to scan all nodes for available data files. These files can be selected and downloaded, and the user can command the nodes to delete those files to free up space on the nodes for additional acquisition events.

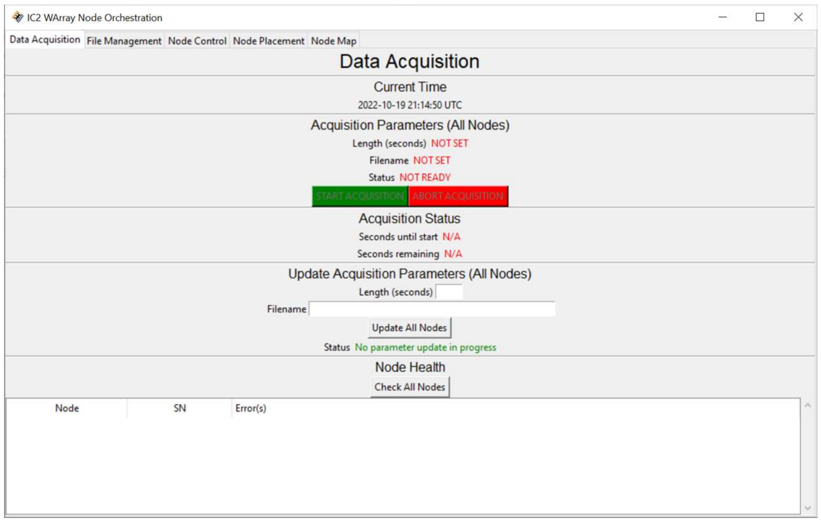

Fig. 10 Data acquisition tab providing control for acquisition settings and triggering.

IV. Experimental Setup

A. Laboratory Testing

All subcomponents of the node were thoroughly tested and characterized prior to deployment. These tests included acoustic testing, time synchronization, environmental testing, and power testing.

1. Acoustic Testing

The dynamic response of the sensor including the sensitivity, linearity, total harmonic distortion (THD), and noise floor are determined using an acoustic wedge, shown in Fig. 11 (a) and (b). An acoustic wedge is a pressure coupler used for comparison calibration/characterization in which a calibrated reference microphone is placed opposite the device under test (DUT). Both the reference microphone and the DUT are flush mounted on opposite walls of a symmetrical wedge-shaped test section. The wedge shape is effective in preventing cavity modes and allows for very high sound pressure levels (SPLs) to ascertain the distortion limit of a DUT. The acoustic source is a BMS 4594ND 1.4" coaxial compression driver with a passive crossover connected to a Crown XLS1502 power amplifier. The calibrated reference microphone used is a 1/4" GRAS, Inc. 46BG condenser microphone with a 184 dB SPL dynamic range upper limit.

The frequency response of the sensor was measured in an infinite tube setup, shown in Fig. 11 (c). The infinite tube apparatus connects an acoustic source to a test section that places a reference microphone and the DUT on opposite sides of a thin symmetrical channel. The test section maintains cross-sectional area while transitioning from a circular inlet and outlet to a 3" (76.2 mm) long, 0.45" (11.5 mm) wide, 0.13" (3.4 mm) tall rectangular cross-section where the microphones are installed flush with the channel surface. The transition to a circular cross-section enables the connection of a 50 ft. (15.2 m) long coiled aluminum tube to the outlet of the test section. This coiled tube approximates an infinitely long tube to nullify the effect of acoustic reflections from the end of the tube that would otherwise impact the frequency response measurement. As with the acoustic wedge, the infinite tube's acoustic source is a BMS 4594ND coaxial compression driver with a passive crossover connected to a Crown XLS1502 power amplifier, and the calibrated reference microphone is a 1/4" GRAS 46BG condenser microphone. This system is capable of testing the acoustic frequency response from 20 Hz to >20 kHz.

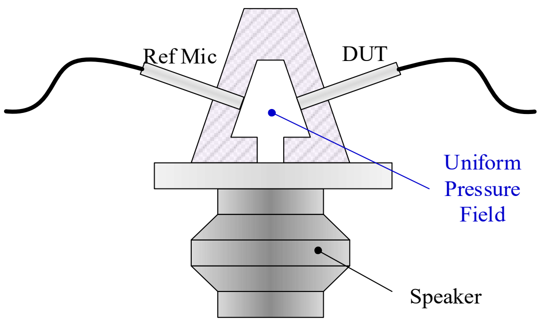

(a)

(b)

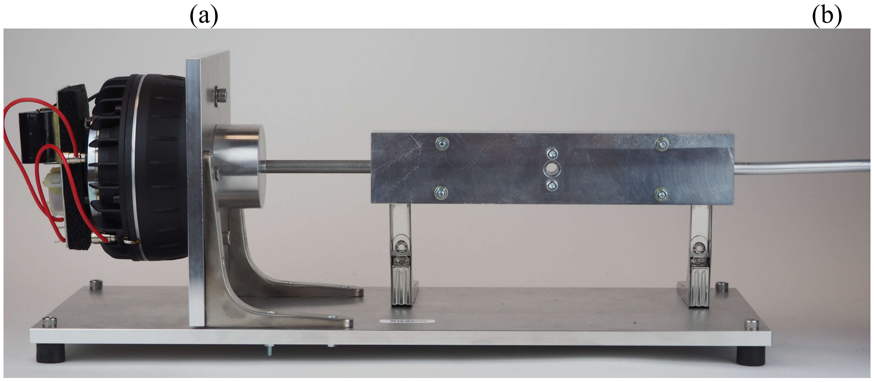

(c)

Fig. 11 (a) Schematic of acoustic wedge design. (b) photograph of acoustic wedge. (c) photograph of thin channel infinite tube (coiled aluminum tube not shown).

2. *Time Synchronization*

To first characterize the ability of the TSM to lock to the GPS signal, a TSM module was positioned with a clear view of the sky and allowed to synchronize for 30 minutes. Once a 'sync' had been achieved, the phase error of the system was recorded and stability and deviation was calculated.

To perform time synchronization testing, two spatially distant wireless nodes were set up outdoors, with a clear view of the sky, and allowed to synchronize their TSMs for ~30 minutes. Then, using a coaxial cable with a tee connection, both nodes were connected to the same function generator using equal-length cables. While the signal generator was producing a 1 kHz, 100 mV input signal, both TSMs were set to trigger at the same future UTC time, and the nodes were programmed to acquire 10 s of data. Once the acquisition was completed the files were downloaded and compared for analysis. This test was then repeated multiple times to build up statistical confidence in the time synchronization.

3. *Temperature Testing*

The satellite nodes should be fully operational over the temperature range of 0°C to 60°C. Testing to confirm this was performed using an environmental chamber on a fully assembled node. Prior to testing, the inputs for microphone channel 0 and microphone channel 1 were shorted together and connected to a single microphone module. The temperature inputs for the two channels were also shorted together and connected to a single microphone module. This ensured the same signal went into both channels of the DAQ and both microphone temperature sensor inputs. The node was placed in the environmental chamber with a GRAS calibrator (with operational specifications spanning the tested range) fastened to the microphone input. A thermocouple was fed through the side of the chamber to monitor the chamber temperature.

The status of the TSM and the temperatures of the chamber, microphone, and battery were recorded while data acquisition was performed. These steps were repeated at temperature set points of 5°C, 15°C, 25°C, 35°C, 45°C, 55°C, and 60°C.

4. IP Testing

The enclosure has undergone the liquid portion of the IP testing and will be tested in the future for solid particle protection. To meet the liquid IPx5 rating, the enclosure should be able to resist ingress from water projected by a 0.25” (6.3mm) nozzle from any direction. The following test parameters are specified for IPx5 enclosures: test duration of 15+ minutes, flow rate of 12.5 liters/minute, and pressure of 30 kPa at a distance of 3 meters.

For this test, a standard 0.5” (1.27 cm) hose connected to an outdoor faucet was used as the water source. A standard 0.5” (1.27 cm) hose has a flow rate of about 34 liters/minute, and the water pressure coming out of a standard faucet is between 275-415 kPa, exceeding the standard test requirements for IPx5 water penetration.

Water indicator tape was placed on the inside of an empty node housing, and then the base and the lid were pressed together and sealed with an O-ring and four screws. The node was taken outside to an open area and tested for water intrusion. While the water was flowing, the node was rotated every 2–3 minutes to ensure all sides of the node were directly in the path of the water jet over the course of the test. After the test, the outside of the node was thoroughly dried, and the lid was removed to inspect for water droplets and discoloration in the moisture indicator tape. Each central plate section also underwent the same water intrusion tests.

B. Array Deployment at NASA Langley

1. Deployment Overview

The array was deployed on a paved runway at the NASA Langley City Environment Range Testing for Autonomous Integrated Navigation (CERTAIN) range [7], shown in Fig. 12(a), for a week in late October 2022. The goal of the deployment was to fully exercise the wireless array functionality in a relevant environment while acquiring noise data for static and moving sources. The choice of late October for the deployment afforded the opportunity to expose the array elements (center plate, satellite nodes, and interface electronics) to the changing weather conditions common to Virginia during this time period. The array design (center plate layout and satellite node locations) was chosen to emulate a subset of a previous array deployed by NASA Langley at Edwards Air Force Base [2]. The array was approximately 50 ft. in diameter, and the control panel was located ~70 ft. off the runway centerline. Test articles included an elevated fixed-point acoustic source positioned at multiple altitudes up to 70 ft. above the array generating both pure tones and band-limited white noise, and a commercial UAS quadcopter both hovering over the center of the array and performing forward flight passes of the array at altitudes up to 70 ft.

The array node locking plates were initially positioned and glued down by using an RTK GPS system that allows for relative positional accuracy of better than 1.4 cm. Once the satellite nodes and central plate were installed, a laser total-station instrument was used to survey the as-deployed positions for greater location accuracy (better than 2 mm). The survey ensured that the positional uncertainty of the microphones was minimized during subsequent acoustic beamforming of the acquired data.

(a) (b)

Fig. 12 (a) Fully deployed wireless array system. (b) variable height stationary noise source (speaker) shown being lifted by a crane. [Source: NASA]

2. Static Source Testing

An elevated acoustic sound source was used as a test article for static excitation of the array. A JBL driver was attached to a 1” interior diameter cylindrical tube with acoustic foam inserted in the end to emulate a pseudo point source. Using a crane (Fig. 12(b)), the source was elevated over the center of the array at heights of 23, 42, and 60 ft. At each height the speaker was driven using a series of pure tones from 250 – 12,000 Hz and band-limited white noise. The array acquired data for 10 seconds for the tones and 20 seconds for the white noise using a sampling rate of 62.5 kHz.

3. Moving Source Testing

To gauge the array’s ability to accurately identify moving noise sources, a commercially available FreeFly AltaX quadcopter, shown in Fig. 13(a), was used. Table 2 shows the relevant dimensions and features of the AltaX. The blade passage frequencies of the propellers provided clearly identifiable sound sources that could be used to verify array capabilities. The flight plan included both static altitude and position hovers, and forward flight passes, both up- and down-range, directly over the center of the array at 32.5 ft/sec, as shown in Fig. 13(b) and (c), respectively. The static hovers and forward flights were performed at altitudes of 30, 50, and 70 ft.

(a)

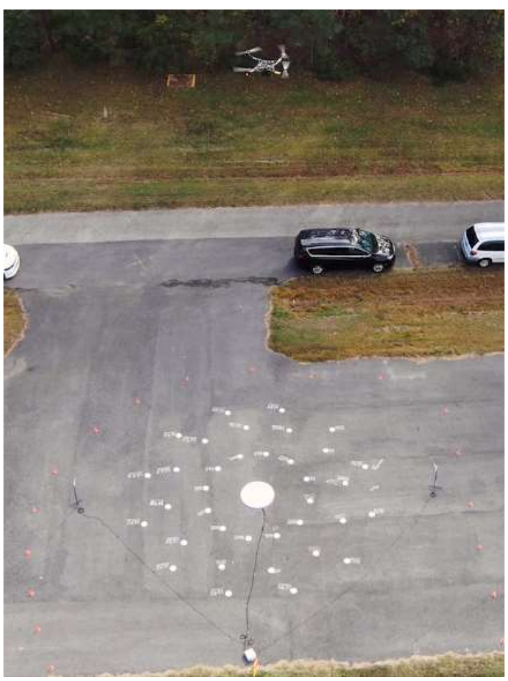

(b)

(c)

Fig. 13 Flyover drone testing. (a) FreeFly Alta X test aircraft. (b) overhead view of AltaX in 50 ft. hover test. (c) ground view of drone flyby at an altitude of 30 ft. [Source: NASA]

Table 2 AltaX Dimensions and Characteristics

UAS Type	Multirotor, 4 brushless motors
MANUFACTURER	Freefly Systems
DIAGONAL LENGTH	55.7 inches (no rotors)
MAXIMUM WEIGHT	76.9 lbs (41.9 lbs with no payload)
LANDING RAILS	None
SPEED	0 – 50.5 knots
ENDURANCE	50 minutes, no payload
COMMAND AND CONTROL	Remote control ground station

V. Testing Results

A. Laboratory Testing

1. Acoustic Testing

82 microphone modules (the 73 intended for initial deployment plus 9 spares) were acoustically tested with the wedge and the infinite tube. It was found that the ±3 dB frequency response of the modules was <10 Hz to 16.9 kHz. 20kHz was within 4dB. An average frequency response graph of all 82 microphone modules is shown in Fig. 14.

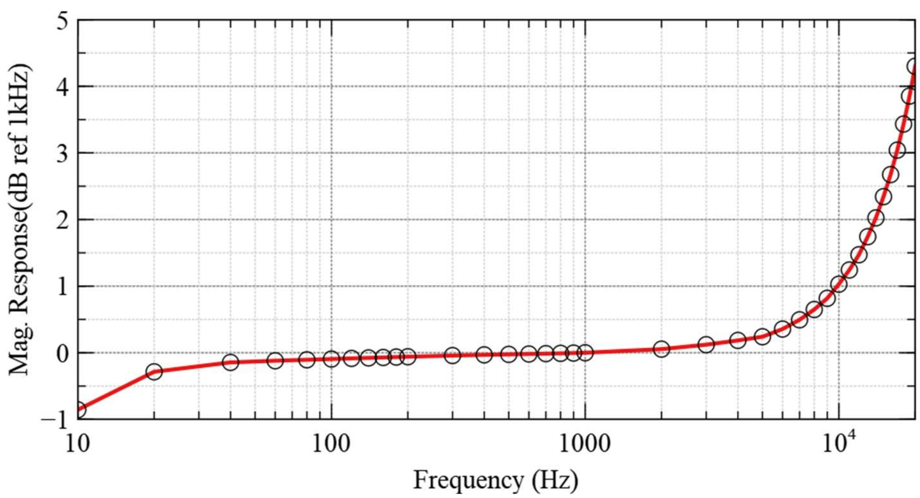

Fig. 14 Average frequency response of microphone module.

Each of the modules was also tested for sensitivity, THD, and noise floor in the acoustic wedge. The histograms of the collected results are shown in Fig. 15 below. The mean performance characteristics of the devices are:

- Sensitivity: 0.7mV/Pa
- THD @ 128 dBSPL: 0.04%
- THD @ 140 dBSPL: 0.11%
- Noise Floor dB (A): 54.1 dBSPL
- Minimum detectable signal @ 1kHz: 16 dBSPL

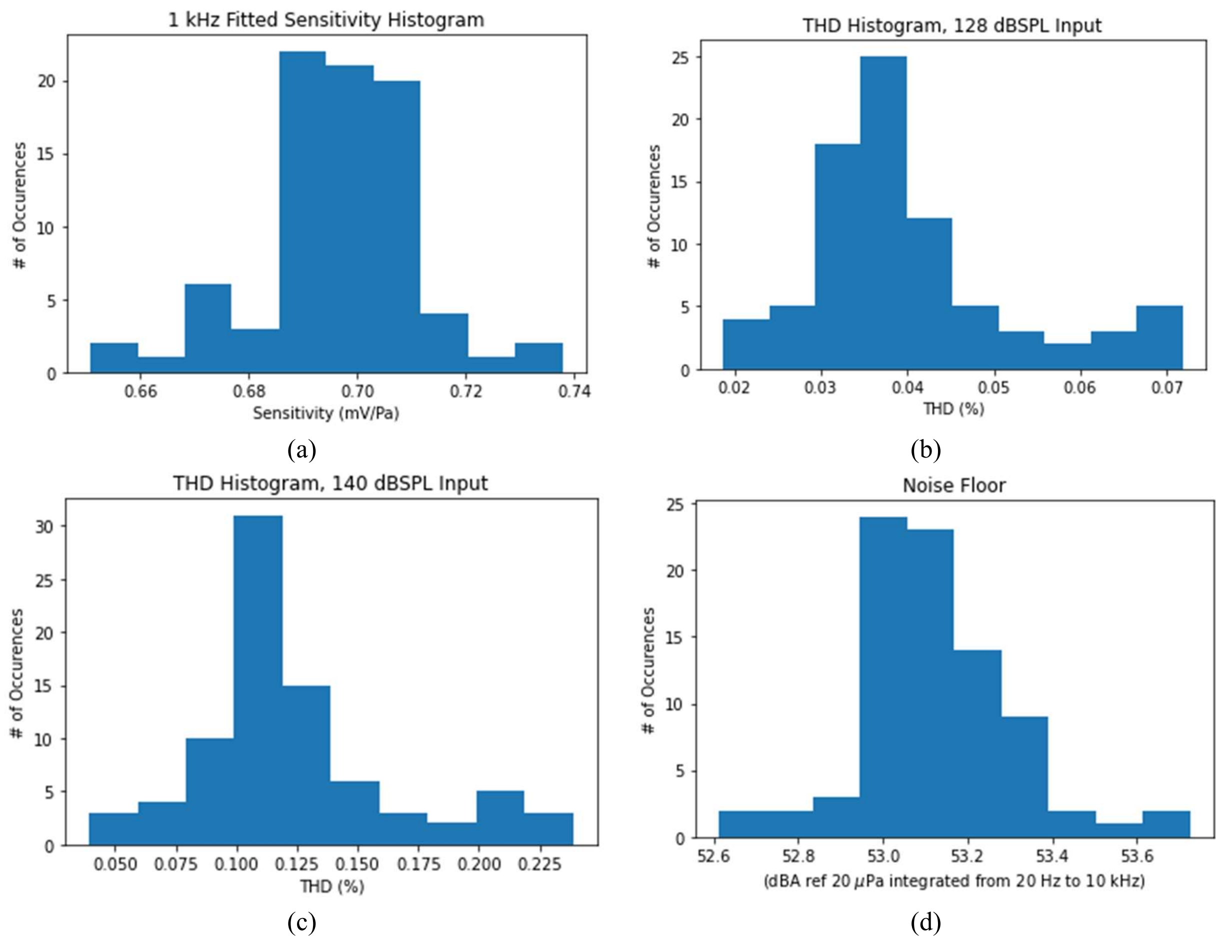

Fig. 15 Histograms representing the performance of all 82 microphone modules assembled.

2. Time Synchronization Testing

The stability of the TSM lock to the GPS signal is as follows:

- Lock time w/ clear sky (±100ns / <40ns): ~ 5 min / ~30 min
- Pulse-per-second clock jitter standard deviation: 3.855 ns
- 10 MHz clock outputs Allan Deviation: < 10e-11
- Worst case holdover time for ±1 µs accuracy: ~3 min

Nominal results for time synchronization between two spatially separated nodes is shown Fig. 16(a). For this test a single function generator signal was applied to both node inputs through use of a tee. The nodes were then allowed to synchronize, and then told to trigger at a specified time. The results show the two signals are essentially indistinguishable, demonstrating the impressive capabilities of a GPS-synchronized, spatially distributed data acquisition system. The same two units were then tested repetitively for 37 acquisitions and the resultant phase difference between the two nodes at 1 kHz is shown in Fig. 16(b). This is an average phase difference is 31 millidegrees which is equivalent to an 86 ns delay. This result is within the initial requirements of 100 ns.

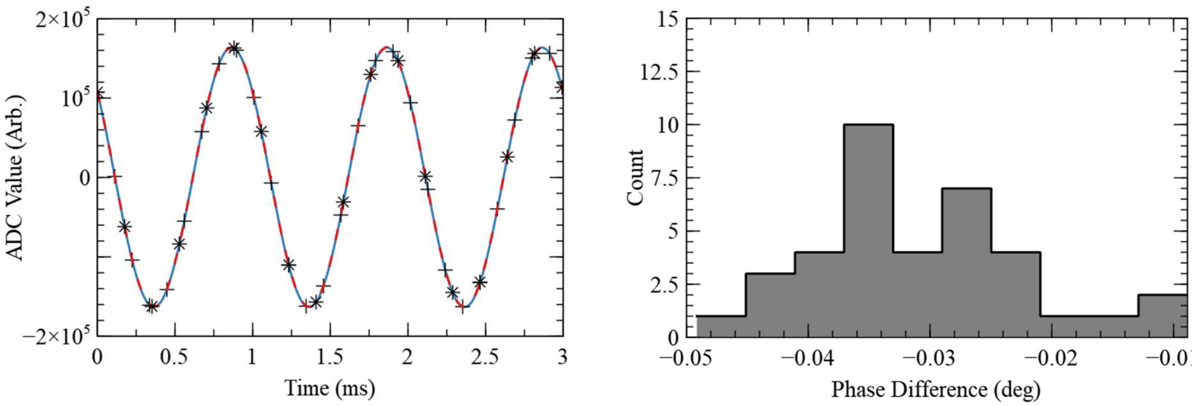

(a) (b)

Fig. 16 (a) Demonstration of time synchronization between two wireless nodes using a 1 kHz, 100 mV input signal. Time histories are shown in blue and red for the two nodes. The y-axis is in ADC arbitrary counts, and the x-axis is in ms. (b) Histogram of phase difference of 37 repeated synchronization tests

3. Temperature Testing

The node is functional over the tested temperature range. The microphone RMS voltage is shown in Fig. 17(a) and is well within the noise of the test system's accuracy. This proves the temperature stability of the ADC system and the MEMS microphone across the required temperature range.

The temperature was also monitored throughout the tests at three points, the results of which are shown in Fig. 17(b): (1) the temperature sensor on the microphone module; (2) the temperature sensor integrated into the battery systems fuel gauge IC on the motherboard; and (3) the air temperature of the chamber. The results show the lowest temperature of the microphone is nominally 12°C even though the actual chamber temperature was lower. At lower temperatures, the heat from the electronics keeps the inside of the satellite microphone enclosure warmer than the environmental chamber temperature. At higher temperatures, the temperature measurement at the microphone module is closer to the chamber temperature, but the battery temperature remains about 3°C warmer than the chamber temperature.

At each measurement point, the data were taken and transmitted to the test engineer over Wi-Fi, thus showing that there were no issues with the communications systems over the entire temperature range. Similarly, the status of the TSM was recorded at each measurement point. At all measurement points, the TSM was able to achieve a time lock with GPS. When the temperature was changed rapidly, such as when the environmental chamber's temperature set point was changed, the TSM's time lock would be momentarily be lost, but when the temperature was changed slowly such as when the chamber's temperature was ramped down at 0.5°C/minute at the end of the test, the TSM maintained its time lock.

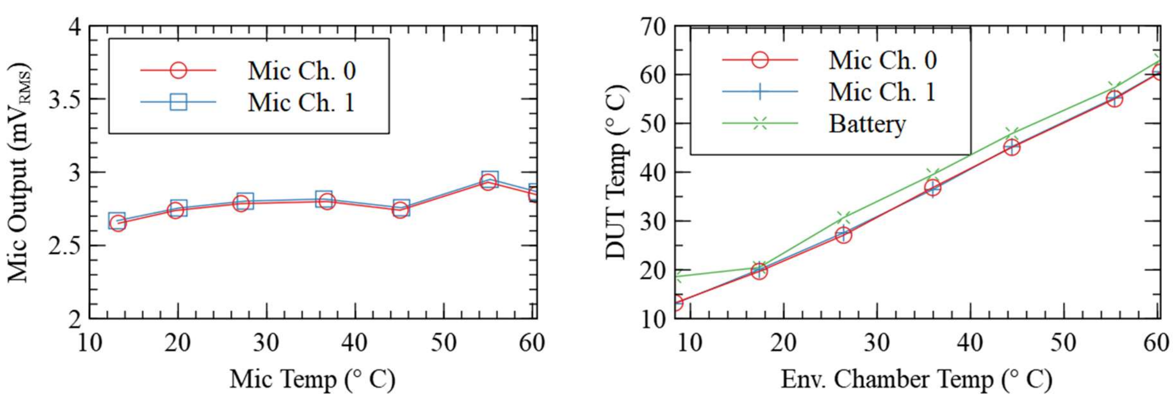

(a) (b)

Fig. 17: (a) Microphone voltage (mVrms) at 1 kHz for microphone channels 0 and 1. (b) microphone and battery temperature vs. environmental chamber temperature.

4. *IP Testing*

After completely drying the outside of the node, it was opened and inspected for water droplets, and it was found that no water entered the node housing during the test. Each central plate section also underwent the same tests and successfully passed without any water intrusion.

B. Array Measurements at CERTAIN Range

1. *Static Source Testing*

The time-history noise data acquired from both the static aerial point source tests and UAS hover runs were processed using conventional frequency-domain beamforming [8]. Cross spectral matrices with a frequency resolution of 7.6 Hz were generated for each dataset, and square Cartesian measurement grids with side dimensions of 240 inches and a spatial resolution of 1.5 inches were generated for the analyses. Due to nonuniformities in the acoustic directivity of the point source at higher frequencies, a simple shading method was employed during the processing of the point source data, using the weights shown in Table 3. The full array was utilized in the processing of UAS hover run data.

Representative conventional beamforming presentations and corresponding theoretical point spread functions for mid-band pure tones generated by the aerial point source are illustrated in Fig. 18. The contour plots have been normalized to the maximum dB value observed over the measurement grid for a given frequency. In general, there is good qualitative agreement between the experimental results and theory, with similar beamwidths and overall sidelobe structures observed. The experimental beamform maps at higher frequencies show elevated sidelobe levels compared with theory. This is not surprising and is due to the acoustic source not representing a pure monopole, coupled with wind effects and extraneous noise sources commonly encountered during outdoor testing.

Table 3 Array Shading Weights Employed for Aerial Point Source Analyses

FREQUENCY (HZ)	MICROPHONE CHANNEL RANGE AND WEIGHT
500	(2:37) = 0, (1, 38:73) = 1
1000	(50:73) = 0, (1:49) = 1
2000	(50:73) = 0, (1:49) = 1
4000	(38:73) = 0, (1:37) = 1
6000	(38:73) = 0, (1:37) = 1
8000	(38:73) = 0, (1:37) = 1
9000	(38:73) = 0, (1:37) = 1
10000	(38:73) = 0, (1:37) = 1

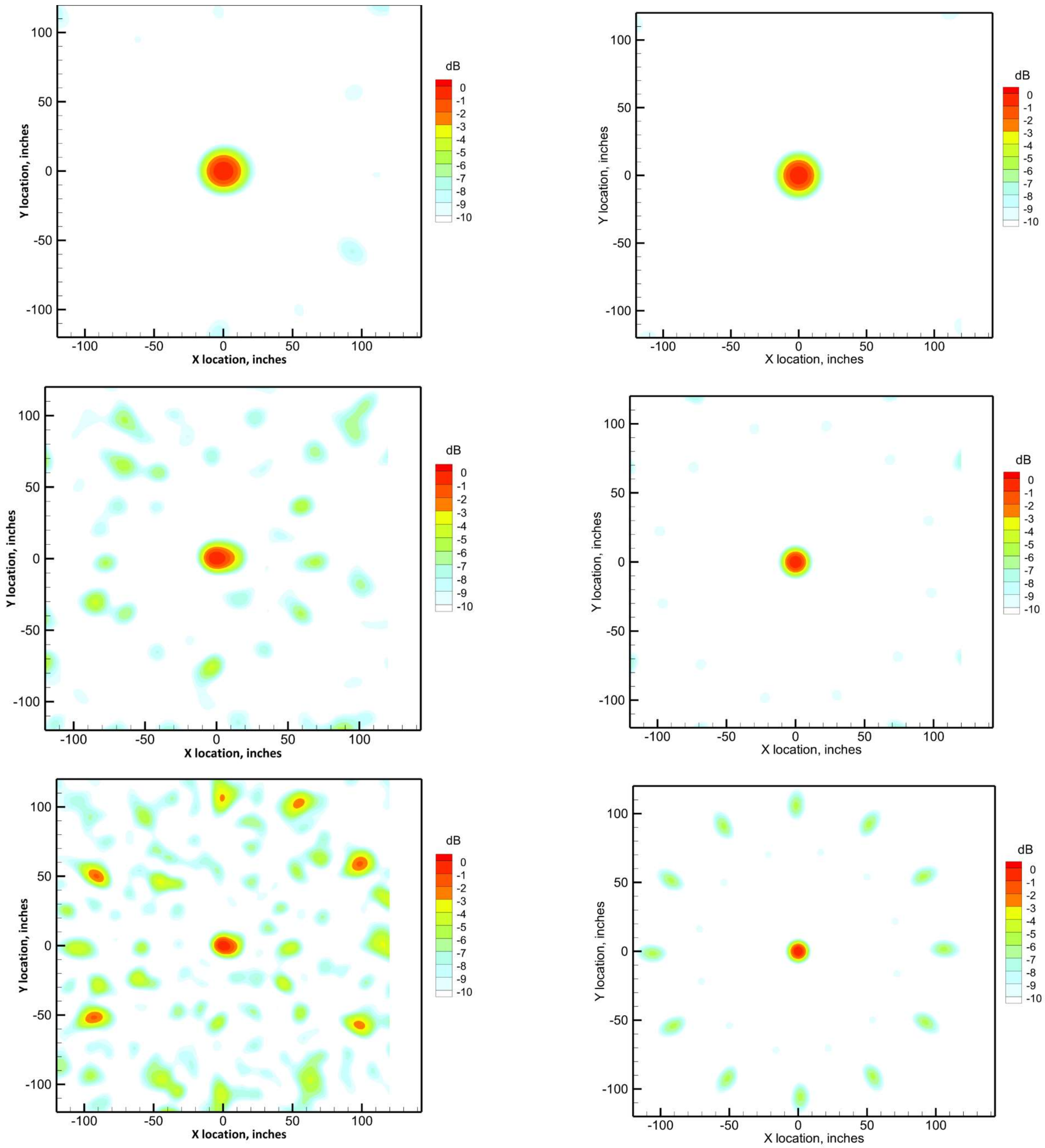

Fig. 18 Comparison of frequency-domain beamform outputs (left) and theoretical point spread functions (right) for a point source located 23 feet above the center of the array.

2. Moving Source Testing

Moving source flyover testing requires the application of time-domain processing techniques that can take into account the amplitude and frequency shifts inherent in the time histories recorded by the individual array microphones. Consequently, time-domain beamforming was employed to produce contour presentations of noise locations and strengths on the UAS vehicle during forward flight operations, using a commercial time domain beamforming code by Avec, Inc.[9] Aircraft position and velocity data were obtained from a GPS tracking system deployed on the vehicle and synchronized with the array system. Typical positional and velocity tracking reports from the aircraft are shown in Fig. 20(a) and (b). A Cartesian measurement grid was generated that encompassed and moved with the noise sources on the vehicle.

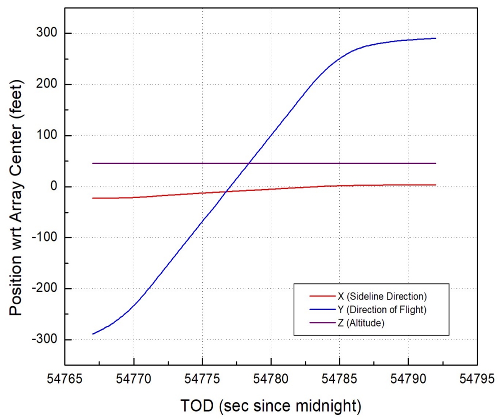

(a)

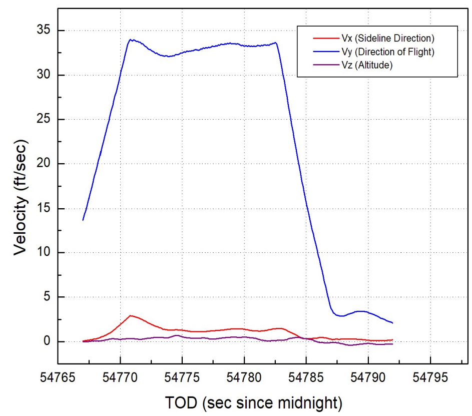

(b)

Fig. 20 (a) A typical GPS positional tracking profile, and (b) a typical GPS velocity tracking profile.

The source location and speed were nominally prescribed using positional and velocity tracking data. For each potential source location (i.e., measurement grid point), the microphone time histories (an example is shown in Figure 19) were resampled with time delays and amplitude adjustments corresponding to a monopole moving at constant velocity in a homogeneous medium, thereby removing the Doppler shift and convective amplification effects [9][10]. No array shading was performed during the time-domain processing.

A comparison of beamform outputs for corresponding hover and forward conditions is shown in Fig. 21. The hover data were processed using the frequency domain beamforming described in Section B.1. while the forward flight data were processed using the time domain technique described above. Vehicle altitudes above ground level were 30 feet for the hover runs and 26 feet for the forward passes, with a constant vehicle speed of approximately 32.5 ft/sec during passage over the center of the array.

Beamform frequencies of 500, 600, and 800 Hz are shown in the figure since these correspond to strong blade passage peaks in the observed autospectra for the array microphones. There are small lateral offsets observed in the forward flight panels in the figure due to uncertainties in the referencing of the flight path to the array center location. Nevertheless, the overall distribution of noise sources on the vehicle is consistent between the hover and forward flight runs. A comparison of the SPL levels between hover and forward flight shows an offset, with higher levels observed for the forward flight runs. Part of this difference can be attributed to the slightly lower altitude of the vehicle during forward flight passes of the array, resulting in a 1.2 dB increase in levels for those runs. The remainder of the

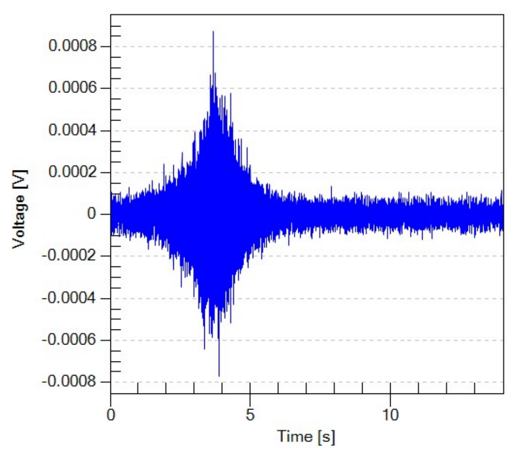

Figure 19: Typical microphone time history for UAS forward flight data capture

[9] http://www.avec-engineering.com/products.html [cited April, 2023]

differences might be attributed to the ambient wind conditions and increased rotor speeds needed for forward flight operation. Nevertheless, the array did an excellent job of capturing the noise from the static and moving vehicle.

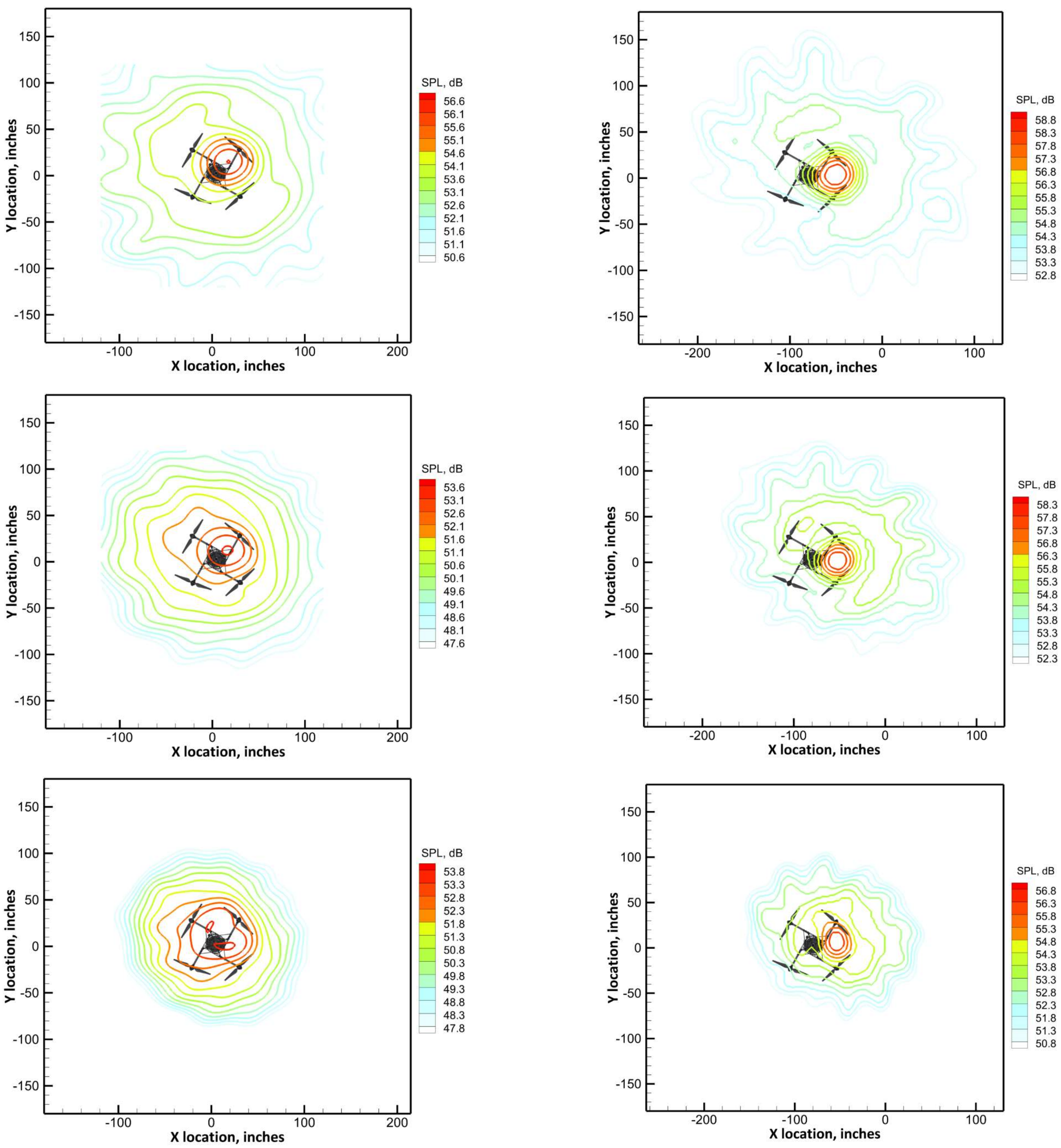

Fig. 21 Comparison of beamform outputs for UAS vehicle in hover (left) and in forward flight (right). Altitude above the array center is 30 feet during hover and 26 feet during forward flight. Forward flight vehicle velocity is approximately 32.5 ft/sec. Top: 500 Hz, Middle: 600 Hz, Bottom: 800 Hz.

VI. Conclusions

This paper presented the design and development of a field-deployable wireless data acquisition system for microphone phased arrays that is suitable for noise-source localization or beamforming measurements such as those encountered during airframe noise flyover measurement tests. The system uses a novel method for wireless time synchronization and data acquisition and environmentally hardened microphones that allow for reduced array hardware and deployment labor costs. These developments will allow for higher fidelity array deployments (e.g., more channels, larger arrays, and multiple array locations) and a greater number of deployments while reducing both equipment acquisition and deployment costs.

A prototype array consisting of 73 microphones was successfully deployed at the NASA Langley Research Center

CERTAIN range and was tested using both an elevated static acoustic source and UAS quadcopter hover runs and fly-over passes of the array. Noise contour presentations generated using conventional frequency-domain beamforming for static sources and time-domain beamforming for moving sources confirmed an excellent ability of the array to detect and characterize the noise generated by a static aerial sound source and a UAS vehicle. Deployment of the array at the CERTAIN range was much faster (less than a day) versus conventional wired arrays (taking several days), and the array was robust to changes in temperature and humidity at the test site. These results validate that the use of a high-channel count wireless array is advantageous in airframe and propulsion noise flyover test campaigns.

Acknowledgments

The authors gratefully acknowledge the support and expertise of the NASA Langley Research Center UAS Operations Office in coordinating the UAS testing conducted on the CERTAIN range. The authors also acknowledge the support of the Langley Center Operations Directorate in providing the use of the crane for static sound source testing of the array.

References

[1] E. R. Waggoner, "An Overview of Lessons Learned from Sonic-boom Flight Research Projects Conducted by NASA Armstrong Flight Research Center," in 2018 Flight Testing Conference, 2018.

[2] W. M. Humphreys, Jr., D. P. Lockard, M. R. Khorrami, W. G. Culliton, R. G. McSwain, P. A. Ravetta, and Z. Johns, "Development and Calibration of a Field-Deployable Microphone Phased Array for Propulsion and Airframe Noise Flyover Measurements," AIAA Paper 2016-2898, 22nd AIAA/CEAS Aeroacoustics Conference, Lyon, France, 2016.

[3] M. R. Khorrami, D. P. Lockard, W. M. Humphreys, Jr., M. M. Choudhari, and T. Van de Ven, "Preliminary Analysis Of Acoustic Measurements From The Nasa-Gulfstream Airframe Noise Flight Test," AIAA Paper 2008-2814, 14th AIAA/CEAS Aeroacoustics Conference, Vancouver, Canada, 2008.

[4] J. R. Underbrink, "Pletharrays for aeroacoustic phased array applications," International Journal of Aeroacoustics, Vols. 16(4-5), pp. 202-229, 2017.

[5] E. A. Baumann, and E. Waggoner, "Flight and Ground Operations in Support of Airframe Noise Reduction Tests," AIAA Paper 2018-2970, 2018 AIAA/CEAS Aeroacoustics Conference, Atlanta, GA, 2018.

[6] T. Schultz, "Finding the boom: Phased array processing applied to sonic boom direction of arrival estimation," International Journal of Aeroacoustics, Vols. 16(4-5), pp. 230-254, 2017.

[7] J. Brown, "CERTAIN: City Environmental Range Testing for Autonomous Integrated Navigation," Presentation to the DOI UAS Interagency Group, 2016.

[8] T. F. Brooks and W. M. Humphreys, Jr., "A Deconvolution Approach for the Mapping of Acoustic Sources (DAMAS) Determined from Phased Microphone Arrays," Journal of Sound and Vibration, Volume 294, pp. 856-879, 2006.

[9] S. Guerin, C. Weckmuller, and U. Michel, "Beamforming and Deconvolution for Aerodynamic Sound Sources in Motion," Proceedings of the Berlin Beamforming Conference (BeBeC), Berlin, Germany, 2006.

[10] A. Dowling, "Convective Amplification of Real Simple Sources," Journal of Fluid Mechanics, Volume 74, Number 3, pp. 529-546, 1976.